# The electrical turn-on characteristics of vertical-cavity surface-emitting lasers

Yang Liu,[a) ] Kent D. Choquette, and Karl Hess

*Department of Electrical and Computer Engineering, University of Illinois at Urbana-Champaign, Urbana, Illinois 61801*

We present a detailed comparison of the electrical turn-on characteristics of 980 nm vertical-cavity surface-emitting lasers (VCSELs) with simulations using a recently extended laser simulator. It is shown that the three recombination mechanisms, spontaneous emission, Shockley–Read–Hall recombination, and Auger recombination, result in distinctly different exponential current–voltage dependencies below threshold. Therefore, information can be extracted about the relative strength of the recombination rates due to those processes, and their relative contributions to the threshold current can be assessed. We show that for the VCSELs studied in this work, spontaneous emission is the dominant contribution to the threshold current. © *2003 American Institute of Physics.* [DOI: 10.1063/1.1628816]

Low threshold current, high wall-plug efficiency, and small temperature sensitivity are desirable in quantum well (QW) laser diode design. These characteristics greatly depend on the electrical efficiency; that is, the ratio of the stimulated recombination rate to the total carrier recombination rate. For small-aperture, oxide-confined, vertical-cavity surface-emitting lasers (VCSELs), there are three important carrier recombination mechanisms that compete with stimulated recombination: spontaneous emission, Shockley–Read–Hall (SRH) recombination, and Auger recombination.[1] It is therefore important to obtain detailed information about these processes so that proper steps can be taken to enhance the electrical efficiency. When VCSELs operate below threshold, the stimulated recombination is negligible, and thus the remaining three recombination channels compose the major portion of the threshold current. These recombination mechanisms exhibit qualitatively different dependencies on the carrier density. As a result, each mechanism is associated with a distinctively different exponential turn-on $I–V$ behavior. Based on this observation, the strength of the recombination mechanisms and their contributions to the threshold current can be determined from detailed (yet simple) measurements of the turn-on $I–V$ characteristics. This approach was previously used to study the surface recombination in light-emitting diodes and laser diodes with bulk active regions.[2,3] Characterization of VCSEL voltage has also been used to quantify the threshold gain[4] and transverse cavity scaling characteristics.[5] In our work, detailed experimental and numerical studies are carried out on VCSELs with QW active regions, and the roles of the three nonstimulated recombination mechanisms are investigated.

It is well known that the exponential turn-on characteristics are completely determined by diffusion and recombination for all $p–n$ junction diodes.[6] For QW laser diodes, however, the QWs represent a very efficient recombination center, and the double heterostructure layers significantly suppress the diffusion of minority carriers into the cladding layers. Therefore, the recombination current in the intrinsic regions [QWs and the separate confinement heterostructure (SCH) layers] gives the most significant contribution to carrier consumption. Furthermore, the carrier injections are laterally confined by the oxide apertures. Hence, contributions from surface recombination at the device perimeters[2,3] are significantly suppressed in our case. The band diagrams of a QW laser diode for both equilibrium and forward bias are illustrated in Fig. 1. With no external voltage applied, the drift and diffusion currents balance each other, and the recombination current is zero due to detailed balance. The two types of carriers therefore have identical quasi-Fermi levels ($F_n = F_p$) which are horizontal throughout the device. The electrons and holes are separated in the $n$- and $p$-doped cladding regions, respectively, by the built-in voltage, and their overlap within the QW is minimal. When a forward bias is applied, the electron and hole quasi-Fermi levels, $F_n$ and $F_p$, respectively, tend to split by the amount equal to the intrinsic
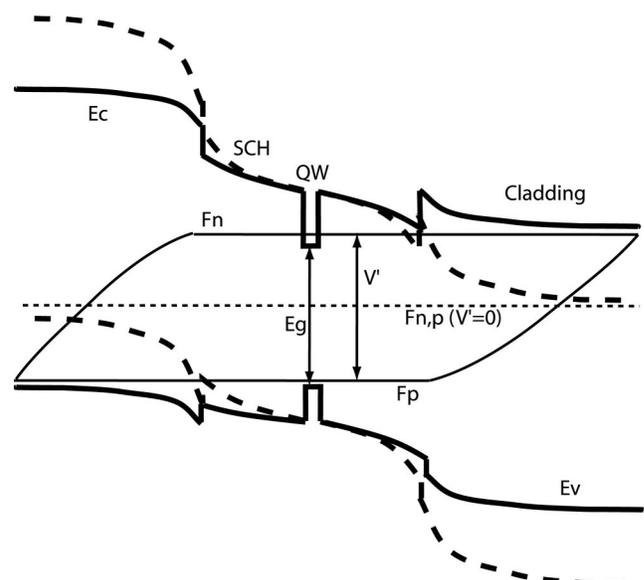


FIG. 1. Schematic plot of band diagrams of a double-heterostructure laser diode operating at thermal equilibrium (dashed line) and forward bias (solid line). $E_{c,v}$ are conduction and valence band edges, and $F_{n,p}$ are electron and hole quasi-Fermi levels, respectively.

[a)] Also at: Integrated Circuits Laboratory, Stanford University, Stanford, CA 94305; electronic mail: yangliu@gloworm.stanford.edu

applied voltage $V'$, which is determined by excluding the voltage drop across the bulk regions from the total external voltage.[4] As a result, the population of both electrons and holes in the QW becomes significant. Under moderate injection conditions, the QW carriers obey Boltzmann statistics. By assuming identical conditions for both carrier types including their band-edge discontinuities, we can express the QW carrier density as $n = p \propto \exp[(V' - E_g)/2k_BT]$, where $E_g$ is the QW bandgap and $k_BT$ is the product of the Boltzmann constant and the carrier temperature. The current component due to the spontaneous emission can then be approximated by $I_{spon} \propto B \cdot n \cdot p \approx B \cdot n^2 \propto \exp[(V' - E_g)/k_BT]$. The current due to the SRH process, that is, due to recombination/generation involving deep-level impurities, is usually modeled by[1]

$$I_{SRH} = \frac{n \cdot p - n_i^2}{\tau_n(n+n_1) + \tau_p(p+p_1)}, \tag{1}$$

where $n_i$ is the intrinsic carrier concentration, $\tau_{n,p}$ are the SRH recombination lifetimes for electron/hole, and $n_1/p_1$ are the electron/hole concentration when the quasi-Fermi level is positioned at the trap energy level. Since $n,p \gg n_i, n_1, p_1$ for moderate injection, we have the corresponding current component $I_{SRH} \approx n \cdot p/(\tau_n n + \tau_p p) \propto \exp[(V' - E_g)/2k_BT]$. $\tau_{n,p}$ may be quite process dependent and range from a few nanoseconds to several hundred nanoseconds. The Auger recombination current is typically modeled by[7]

$$I_{Aug} = C_n \cdot n^2 \cdot p + C_p \cdot n \cdot p^2. \tag{2}$$

The Auger coefficients $C_{n,p}$ account for processes where the second electron/hole gains the energy, respectively. Usually, $C_n$ is much smaller than $C_p$. Based on the same assumptions as made earlier, we approximately have $I_{Aug} \propto \exp[(3/2)(V' - E_g)/k_BT]$. The importance of the Auger process depends strongly on the material system, and there is a wide range for $C_p$: $3.5 \times 10^{-30} - \sim 0.9 \times 10^{-28}$ cm$^6$s$^{-1}$ for GaAs and InGaAsP QWs operating between 850 and $\sim 1550$ nm.[7] When the carrier injection is high, so that the lasing threshold is approached, the power law dependence of the recombination current on the carrier density is still valid. However, the QW carriers become degenerate and the use of the Fermi–Dirac distribution function becomes necessary. The QW carrier density then increases as $\Delta n \propto \Delta[(V' - E_g)/2k_BT]$, and therefore the recombination currents tend to deviate from their exponential dependence on $V'$.

In order to quantify the approximate analysis just presented, we have performed detailed electrical measurements as well as comprehensive device level simulations for 980 nm VCSELs with double-oxide confined apertures.[4] The active region consists of three 80 Å InGaAs QWs. The cavity is of $1 - \lambda$ thickness and the SCHs are composed of linearly graded AlGaAs. The QWs and SCHs are undoped, but the oxide apertures are moderately doped at a density of $10^{18}$ cm$^{-3}$. The size of the square oxide aperture is 4.5 $\times 4.5$ $\mu$m$^2$. An Agilent 4156 semiconductor parameter analyzer has been used to obtain $I-V$ measurements. The simulation work is based on MINILASE laser diode simulator, which models the carrier transport and various recombination mechanisms in detail[8] and also computes the QW band
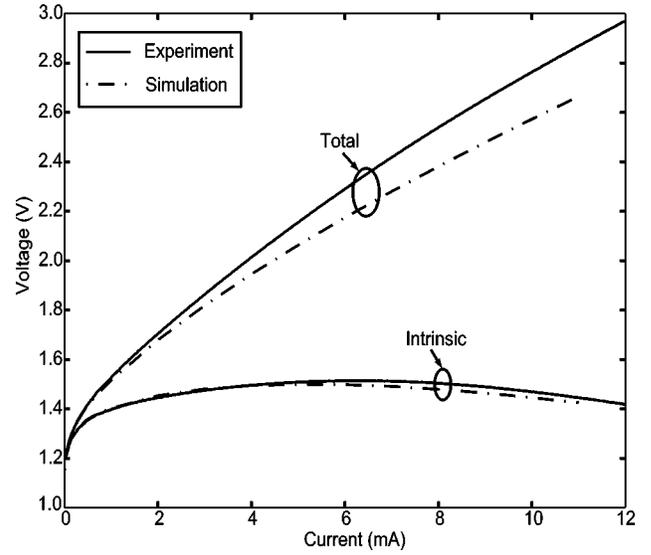


FIG. 2. Measured and simulated total and intrinsic voltage as functions of injection current into a 980 nm VCSEL.

structure by using an eight-band $\mathbf{k} \cdot \mathbf{p}$ method.[9] In MINILASE, the QW spontaneous emission current is carefully modeled as

$$I_{spon} \propto \int_0^\infty d\omega Z(\omega) \int_0^\infty d\omega' L(\omega, \omega') r^0(\omega'), \tag{3}$$

where $Z(\omega)$ is the photon density of states at angular frequency $\omega$, and $L(\omega, \omega')$ is a Lorentzian-type broadening function. The unbroadened spontaneous emission density rate $r^0(\omega)$ is expressed as

$$r^0(\omega) \propto \sum_{i,j} \sum_{\mathbf{k}} |M_{c,v}^{i,j}|^2 \delta(E_{c,\mathbf{k}}^i - E_{v,\mathbf{k}}^j - \hbar\omega)$$
$$\times f_c(E_{c,\mathbf{k}}^i) f_v(E_{v,\mathbf{k}}^j), \tag{4}$$

where the summations go over conduction and valence subbands and k-space, $M_{c,v}^{i,j}$ is the optical matrix element, $f_c$ and $f_v$ are electron and hole occupation factors, respectively, obeying Fermi–Dirac statistics, and the $\delta$-function is for energy conservation. The SRH and Auger recombination processes are modeled by Eqs. (1) and (2), but the realistic QW band structure as well as Fermi–Dirac statistics are used for computing the carrier density.

The measured and simulated $I-V$ curves are shown in Fig. 2. The series resistance associated with the top and bottom distributed Bragg reflectors (DBRs) contributes to the device voltage drop, which is included in the measurement of the total voltage $V$. MINILASE models the DBR stacks as bulk regions with artificially low mobilities. In Fig. 2, the difference in the slope of the $I-V$ curve between experiment and simulation corresponds to $\sim 16$ $\Omega$ series resistance. This difference is likely due to the contact and substrate series resistance, which is not included in the simulation.

The intrinsic voltage across the QWs is the principle interest in this work, and it is not affected by the value of series resistance. The intrinsic voltage is calculated as $V' = V - IR_s$, where the series resistance $R_s$ is obtained from linear fitting of the $I-V$ curve above the threshold.[4] The $I-V'$ curve is also plotted in Fig. 2 for both experiment and simulation, and a good agreement is observed. The exponential $I-V'$ dependence is evident below laser threshold
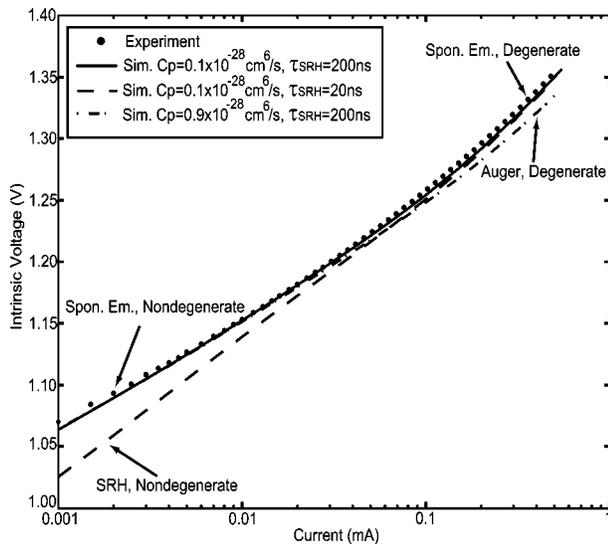
FIG. 3. Measured and simulated turn-on current and intrinsic voltage dependence. Different recombination parameters are used in the simulations.
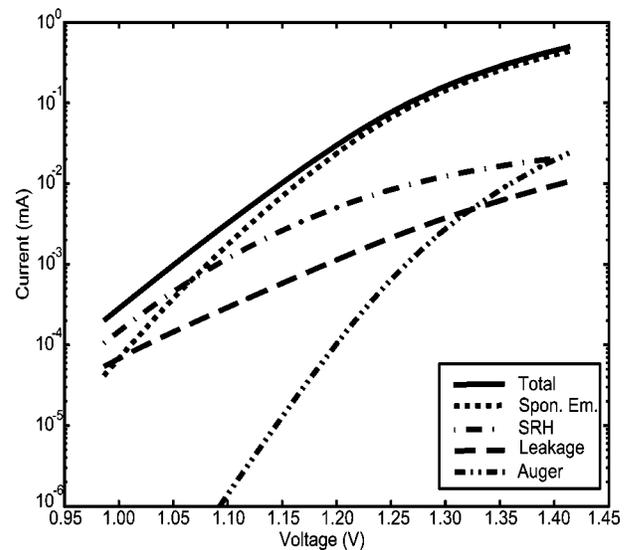


FIG. 4. Simulated current components associated with various recombination mechanisms against the total voltage bias below the threshold. In the simulation, $C_p = 0.1 \times 10^{-28}$ cm$^6$s$^{-1}$ and $\tau_{SRH} = 20$ ns.

($\sim$0.7 mA for this sample), and $V'$ is almost pinned due to strong stimulated recombination above the threshold. It is shown in Fig. 2 that $V'$ actually decreases by a small amount when the operating current rises to very high values. This is probably caused by the bandgap shrinkage because the QWs are heated up at higher bias. The self-heating effects are negligible below the threshold.

Figure 3 shows the turn-on $I–V'$ characteristics, as obtained from detailed measurements as well as simulations including different SRH and Auger recombination rates, which vary by an order or more of magnitude. The simulation shows excellent agreement with the experimental results when SRH and Auger recombination rates are set to be small ($\tau_n = \tau_p = \tau_{SRH} = 200$ ns and $C_p = 0.1 \times 10^{-28}$ cm$^6$s$^{-1}$). In this case, the spontaneous emission is the dominant process that contributes to the threshold current. If an ideality factor $n$ is introduced to characterize the exponential dependence so that $I \propto \exp[(V' - E_g)/nk_BT]$, we have $n \approx 1.3$ when QW carriers are nondegenerate. As the carrier injection increases and QW carriers become degenerate, a deviation from the exponential dependence is clearly observed. If we increase the QW SRH recombination rate in the simulation to $\tau_{SRH} = 20$ ns, the resultant $I–V'$ curve shows qualitatively different behavior at low bias ($n \approx 2$), as shown in Fig. 3. This is attributed to the significant contribution from SRH recombination for low carrier densities. Similar features are also observed if we take $\tau_{SRH} = 200$ ns, but reduce the SRH lifetime in the SCH regions. If we increase the Auger coefficient to $C_p = 0.9 \times 10^{-28}$ cm$^6$s$^{-1}$ while keeping the SRH rate small, the $I–V'$ curve still agrees with the experimental data at low and moderate carrier injection. Nevertheless, an overshoot of the current is evident at high carrier injection as shown in Fig. 3, which is due to the appreciable Auger current.

Simulated current components below threshold are plotted in Fig. 4 versus the bias voltage. A distinctively different exponential dependence is clearly shown to be associated with each recombination current type. The leakage current is also plotted in this figure, whose dominant component is from the SRH recombination in the SCH regions. This is because the carrier injection within the SCH regions is small

due to the wide bandgap. It is also shown in Fig. 4 that the SRH current plays a relatively larger role at low carrier densities while the opposite is true for the Auger current. Therefore, contributions of different recombination processes to the threshold can be evaluated from the turn-on $I–V$ behavior. It can be concluded from Fig. 3 that the spontaneous emission current is the dominant threshold component for the VCSEL samples used in this study.

In summary, we have studied the electrical turn-on characteristics of VCSELs both experimentally and by simulation. We have demonstrated that distinctively different current–voltage dependencies are associated with spontaneous, SRH, and Auger recombination processes. Based on this observation, the influences of these recombination mechanisms on the VCSELs' threshold current are investigated. This approach enables extraction of important information on optical and thermal properties of laser diodes from direct electrical measurements. It is also expected to be useful in characterizing the crystal quality of QWs and SCH regions in laser diodes.

[1] K. Hess, *Advanced Theory of Semiconductor Devices* (IEEE, Piscataway, NJ, 2000), and references therein.
[2] C. H. Henry, R. A. Logan, and F. R. Merritt, Appl. Phys. Lett. **31**, 454 (1977).
[3] M. Fukuda, J. Appl. Phys. **59**, 4172 (1986).
[4] K. D. Choquette, W. W. Chow, K. M. Geib, and R. P. Schneider, Jr., Appl. Phys. Lett. **68**, 3689 (1996).
[5] K. D. Choquette, W. W. Chow, G. R. Hadley, H. Q. Hou, and K. M. Geib, Appl. Phys. Lett. **70**, 823 (1997).
[6] S. M. Sze, *Semiconductor Devices: Physics and Technology*, 2nd ed. (Wiley, New York, 2002).
[7] L. A. Coldren and S. W. Corzine, *Diode Lasers and Photonic Integrated Circuits* (Wiley, New York, 1995), and references therein.
[8] M. Grupen and K. Hess, IEEE J. Quantum Electron. **34**, 120 (1998).
[9] F. Oyafuso, P. von Allmen, M. Grupen, and K. Hess, VLSI Design **8**, 463 (1998).